

Dark Energy Tomography

Yong-Seon Song* and Lloyd Knox†

Department of Physics, One Shields Avenue, University of California, Davis, California 95616

(Dated: November 4, 2018)

We study how parameter error forecasts for tomographic cosmic shear observations are affected by sky coverage, density of source galaxies, inclusion of CMB experiments, simultaneous fitting of non-dark energy parameters, and the parametrization of the history of the dark energy equation-of-state parameter $w(z)$. We find tomographic shear-shear power spectra on large angular scales ($l < 1000$) inferred from all-sky observations, in combination with Planck, can achieve $\sigma(w_0) = 0.06$ and $\sigma(w_a) = 0.09$ assuming the equation-of-state parameter is given by $w(z) = w_0 + w_a(1 - a(z))$ and that nine other matter content and primordial power spectrum parameters are simultaneously fit. Taking parameters other than w_0 , w_a and Ω_m to be completely fixed by the CMB we find errors on w_0 and w_a that are only 10% and 30% better respectively, justifying this common simplifying assumption. We also study ‘dark energy tomography’: reconstruction of $w(z)$ assumed to be constant within each of five independent redshift bins. With smaller-scale information included by use of the Jain & Taylor ratio statistic we find $\sigma(w_i) < 0.1$ for all five redshift bins and $\sigma(w_i) < 0.02$ for both bins at $z < 0.8$. Finally, addition of cosmic shear can also reduce errors on quantities already determined well by the CMB. We find the sum of neutrino masses can be determined to ± 0.013 eV and that the primordial power spectrum power-law index, n_S , as well as $dn_S/d\ln k$, can be determined more than a factor of two better than by Planck alone. These improvements may be highly valuable since the lower bound on the sum of neutrino masses is 0.06 eV as inferred from atmospheric neutrino oscillations, and slow-roll models of inflation predict non-zero $dn_S/d\ln k$ at the forecasted error levels when $|n_S - 1| > 0.04$.

PACS numbers: 98.65.Dx, 98.70.Vc, 95.35.+d, 98.80.Es

I. INTRODUCTION

The great mystery of twenty-first century cosmology is the dark energy—a smooth, negative-pressure component evoked to bring the Universe to critical density (e.g., [1, 2]) and to dim high-redshift supernovae [3, 4, 5]. Observers are constraining, or planning to constrain, this curious component in a number of ways, both through its influence on structure formation and on geometry. Here we consider how well the component can be probed by tomographic cosmic shear observations of large-scale structure.

Cosmic shear is a very promising technique for studying the large-scale structure and constraining the cosmological parameters that govern its evolution. For a recent review see [6]. The shear signal only depends on the mass distribution; it is immune to uncertainties in the relationship between mass and light that plague other observations. On large scales, given a model, the statistical properties of this mass distribution can be calculated with very high accuracy, thus there is a well-understood relation between theory and observable.

Cosmic shear also naturally probes the chief redshift range of interest for constraining dark energy: $0 < z < 2$. In this redshift range, dark energy becomes the dominant contributor to the energy density and thus has significant effect on the expansion rate, $H(z)$. The expansion rate

affects the shear power spectrum both through its effect on the growth rate and also by altering how length scales at a given redshift project into angular scales. At $z > 2$, for the simplest models, the dark energy is highly subdominant and has little influence on structure formation.

Multi-band photometry makes possible tomographic cosmic shear, in which source galaxies are binned according to their photometrically-determined redshifts, and separate shear maps are made for each source galaxy redshift bin. This technique allows one to study the evolution of the density field as a function of redshift, restoring the information otherwise lost by projection over the broad lensing kernel.

Many papers [7, 8, 9, 10, 11, 12, 13, 14, 15] have studied how well tomographic shear correlations can be used to constrain dark energy parameters. All but one of these error forecasts [7] were done in the limit of other cosmological parameters being perfectly known *a priori*. This assumption is justified if CMB (or other) observations can be used to determine the parameters with negligibly small errors. We investigate this assumption by letting eight other cosmological parameters float, constrained only by the cosmic shear data themselves and various CMB observations. For WMAP, Planck, and a future polarization satellite described below we find the constraints on the dark energy parameters degrade by 70%, 30% and 4% respectively.

We parametrize the time-dependence of w in two different ways. First, following Linder [16], we write $w(z) = w_0 + w_a(1 - a(z))$. This parametrization has the advantage of tending toward a constant at high redshift, preventing high-redshift dark energy dominance that can

*Electronic address: yssong@bubba.ucdavis.edu

†Electronic address: knox@bubba.ucdavis.edu

occur with the parameterization $w(z) = w_0 + w_z z$. It is therefore a convenient parametrization when combining $z < 2$ observations with $z \simeq 1100$ CMB observations.

Weller & Albrecht [17] have argued that all models in the literature can have their luminosity distances as a function of redshift fit by the $w(z) = w_0 + w_z z$ parametrization to 1% accuracy in the $0 < z < 2$ range. However, dark energy is so poorly understood that it is worth considering $w(z)$ histories that do not occur in any existing scalar field quintessence models. Therefore we also study a less model-dependent parameterization, one in which $w(z)$ is constant within each of five independent redshift bins. An approach somewhat similar to ours is that of [18] who parametrized $w(z)$ with its principal components, given supernovae data as expected from the Supernova/Acceleration Probe (SNAP). We have found that data that give similar constraints in the w_0, w_a plane may give strikingly different constraints in the space of redshift bins of w .

In this paper we concentrate on what is possible with the data on large angular scales where theoretical interpretation is most straightforward. There is also great potential for data on smaller angular scales although the state of theory must be improved to take full advantage of it. Potentially great use can be made of two and three-point functions out to $l = 10^5$ (e.g., [10]). Even at $l < 3000$, including the 3-point function can improve errors by a factor of 3 [11]. Counting of mass clusters is another promising way to exploit the small angular scale data [19].

We do consider one method of using the small angular scale data here. Recently [20] and [21] have proposed using the data in such a way as to be insensitive to the uncertain fluctuation statistics and only dependent on easily-calculated geometric quantities. We combine a conservative use of the ratio statistic of [20] with the large angular scale shear-shear power spectra. We find that the addition of the ratio statistic greatly improves our reconstruction of $w(z)$ even with a conservative forecast of how well the ratio statistic can be measured.

In addition to dark energy, another exciting application of high-precision cosmic shear data is to determine the mass of the relic neutrinos. In the first cosmic shear + CMB forecasting papers, [22, 23] it was shown that combining Planck and all-sky cosmic shear could determine the sum of the masses of the different flavors of relic neutrinos to 0.02 eV with w fixed to -1. Recently [24] showed that a post-Planck all-sky CMB polarization mission could be used to determine the sum to 0.04 eV without cosmic shear data. The sum is at least 0.06 eV in order to explain atmospheric neutrino oscillations [25] hence a detection is assured, though possibly one of weak statistical significance. Here we show that all-sky CMB polarization observations combined with all-sky weak lensing observations can reduce this error to 0.027 eV or, with the inclusion of the ratio statistic, to 0.013 eV even with simultaneous determination of w_0 and w_a . This reduction in error may change a two σ detection

to a five σ detection.

We discuss the shear-shear correlations in section II and the binning of the dark energy history in section III. In section IV we discuss the parameters of the future weak lensing and CMB experiments we consider and in section V outline our error-forecasting method. In section VI we give results for constraints on the dark energy and neutrino mass and all the other cosmological parameters we assume our simultaneously fit. In section VII we see how the results improve with the addition of the ratio statistic.

II. TOMOGRAPHIC COSMIC SHEAR-SHEAR CORRELATIONS

The size and shape of galaxies is altered by gravitational lensing. The effect of lensing is described by the 2×2 transformation matrix A_{ij} given by

$$A_{ij} \equiv \frac{\partial \theta_s^i}{\partial \theta^j} = \begin{pmatrix} 1 - \kappa - \gamma_1 & \gamma_2 \\ \gamma_2 & 1 - \kappa + \gamma_1 \end{pmatrix}. \quad (1)$$

where θ_s is the angular location in the source plane for a light ray appearing at θ in the image plane. The convergence κ describes the magnification or demagnification while the shear components, γ_1 and γ_2 , quantify the distortion of the shape [26, 27].

The shear components can be inferred from measurement of galaxy ellipticities. Galaxies have their own intrinsic ellipticity and an additional ellipticity due to lensing so that

$$\mathbf{e}^\mu = \mathbf{e}^{\mu}_{\text{int}} + \mathbf{e}^{\mu}_{\text{lens}} \quad (2)$$

where μ labels the galaxy. The average shear in a pixel on the sky can be estimated from averaging over the galaxies in the pixel:

$$\begin{aligned} \gamma_1 &= \frac{1}{2N_{\text{pix}}} \sum_{\mu} e^{\mu}_{+} = \frac{1}{2N_{\text{pix}}} \sum_{\mu} (e^{\mu}_{+, \text{int}} + e^{\mu}_{+, \text{lens}}) \\ \gamma_2 &= \frac{1}{2N_{\text{pix}}} \sum_{\mu} e^{\mu}_{\times} = \frac{1}{2N_{\text{pix}}} \sum_{\mu} (e^{\mu}_{\times, \text{int}} + e^{\mu}_{\times, \text{lens}}) \end{aligned} \quad (3)$$

where $+$ and \times denote the two orthogonal ellipticity components. In the absence of correlations between the intrinsic ellipticities, the rms error in the measurement of each shear component is

$$\sigma(\gamma_1) = \sigma(\gamma_2) = \gamma_{\text{rms}} / \sqrt{N_{\text{pix}}} \quad (4)$$

where γ_{rms} is the rms intrinsic shear of the galaxies and N_{pix} the number of galaxies in the pixel.

Maps of the shear components can be decomposed into even parity E modes and odd parity B modes, just as is the case with linear polarization Stokes parameters, Q and U [28, 29]. Assuming uniform coverage, the noise in the E modes will have a diagonal covariance matrix \mathbf{N} given by

$$N_{lmB, l'm'B'} = N_l^B \delta_{ll'} \delta_{mm'} \delta_{BB'}. \quad (5)$$

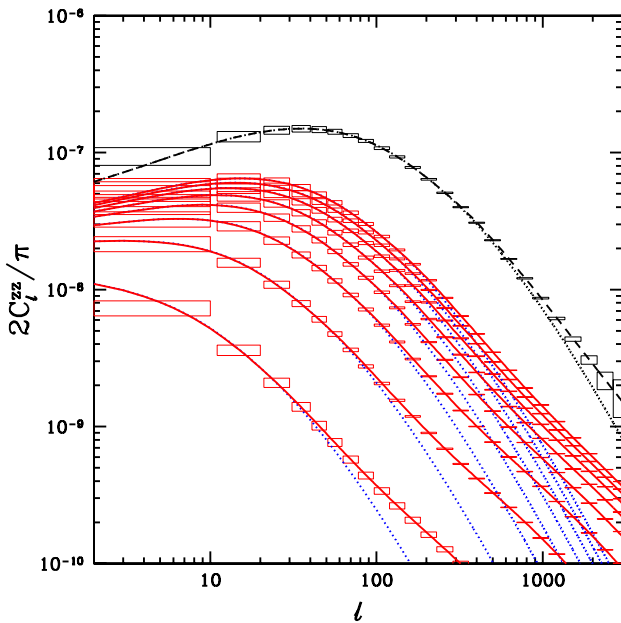


FIG. 1: The shear-shear auto power spectra. The 8 solid curves are the shear power spectra from each of the galaxy source planes, B_1 to B_8 . Dotted curves are the linear perturbation theory approximation. From bottom to top the source plane redshift ranges are B_1 : $z \in [0.0, 0.4]$, B_2 : $z \in [0.4, 0.8]$, B_3 : $z \in [0.8, 1.2]$, B_4 : $z \in [1.2, 1.6]$, B_5 : $z \in [1.6, 2.0]$, B_6 : $z \in [2.0, 2.4]$, B_7 : $z \in [2.4, 2.8]$ and B_8 : $z \in [2.8, 3.2]$. The error boxes are forecasts for G4 π (see Table I). The top dashed curve is the shear power spectrum for the CMB source plane. The error boxes are forecasts for CMBpol (see Table II).

where

$$N_l^B = \gamma_{\text{rms}}^2 \Omega_{\text{pix}} / N_{\text{pix}}^B \quad (6)$$

and B labels the source redshift bin. The signal contribution to the covariance of the shear E modes, S , is correlated across bins, but otherwise diagonal:

$$S_{lmB,l'm'B'} = C_l^{BB'} \delta_{ll'} \delta_{mm'}. \quad (7)$$

The shear angular power spectra are given by

$$C_l^{BB'} = \frac{\pi^2 l}{2} \int dr r W^B(r) W^{B'}(r) \Delta_{\Phi}^2(k, r) \quad (8)$$

where the window function for sources in redshift bin, B , is

$$W^B(r) = \frac{1}{\bar{n}_B} \frac{2}{r} \int_{r(z_{\text{min}}^B)}^{r(z_{\text{max}}^B)} dr' \frac{(r' - r)}{r'} N_B(z') dz' / dr' \Theta(r' - r), \quad (9)$$

and the average number density of galaxies in redshift bin B is

$$\bar{n}_B = \int_{r(z_{\text{min}}^B)}^{r(z_{\text{max}}^B)} dr' N_B(z') dz' / dr'. \quad (10)$$

We use Peacock and Dodds' formulation [30] to calculate the non-linear density power spectrum, $\Delta_{\Phi}^2(k, r)$. We only use data with $l < 1000$ to reduce our sensitivity to errors in the non-linear corrections and departures from Gaussianity [31].

We assume that photometrically-determined redshifts can be used to sort the source galaxies into eight redshift bins with $\Delta z = 0.4$ from $z = 0.0$ to $z = 3.2$. The shear power spectra for these eight source bins are shown in Fig. 1. The higher the source bin redshift, the higher the shear power. The shear power spectra are related to the deflection angle power spectra by

$$l(l+1)C_l^{dd}/(2\pi) = 2C_l^{\gamma\gamma}/\pi \quad (11)$$

thus the area under the curves in Fig. 1 gives the contribution to the deflection angle variance from a given range of l . The expected errors on the auto power spectra are given by

$$\Delta C_l^{BB} = \sqrt{\frac{2}{(2l+1)f_{\text{sky}}}} (C_l^{BB} + N_l^{BB}). \quad (12)$$

Shear maps can also be inferred from observations of CMB temperature and polarization. The top curve in Fig. 1 is the shear power spectrum for sources at $z \sim 1100$. The auto and cross-correlation (with the eight other shear maps) power spectra for the CMB shear map is also given by Eq. 8. However, the window function, due to the small thickness of the last-scattering surface is simply given by

$$W^{\text{CMB}}[r(z)] = \frac{r(z_s) - r(z)}{r(z_s)r(z)} \quad (13)$$

where z_s is the redshift of the last-scattering surface, defined as the peak of the visibility function. We calculate the error in the reconstructed shear maps using the quadratic estimator of [32]. The noise level in Fig. 1 is for the CMBpol experiment described in section IV. At these noise levels, a maximum-likelihood shear map would have up to two times lower reconstruction noise than the quadratic estimator shear map [33].

Thus we have grouped the data into nine different redshift bins for lensing tomography: eight bins with galaxies as the sources (from $z = 0.0$ to $z = 3.2$) and a ninth bin on the CMB last-scattering surface.

III. BINNING DARK ENERGY HISTORY

We parametrize the history of the dark energy equation of state parameter as

$$w(z) = \sum_i \chi_i(z) w_i \quad (14)$$

where

$$\chi_i(z) = \begin{cases} 1 : & z_{\text{min}}^i < z < z_{\text{max}}^i \\ 0 : & \text{otherwise.} \end{cases} \quad (15)$$

We define 5 bins: 4 bins with equal redshift spacing $\Delta z = 0.4$ and the last bin from $z = 1.6$ to the last scattering surface. We choose this binning because the data are sufficiently powerful to place interesting constraints on this space. Finer binning, particularly beyond $z = 1.6$, would lead to very strong degeneracies between the bins.

Note that the discrete parametrization of the dark energy equation-of-state parameter is well-matched with what we observe in weak lensing experiments with binned source planes. The variation of w_i in bin i influences the dark energy density in all the lower redshift bins. Likewise, the shear map from galaxies in bin i are affected by the large-scale structure in those same lower redshift bins.

This discrete binning of $w(z)$ does lead to complications on very large scales where dark energy density fluctuations can be important. While it is straightforward to calculate the expansion rate and therefore distance as a function of redshift for $w(z)$ given by Eq.(14), it is not clear how to calculate the fluctuations in the dark energy density and pressure for a model with non-continuous $w(z)$. On small scales, the dark energy fluctuations (at least for the simplest scalar-field models) are damped out. The critical scale k_Q (l_Q in harmonic space) is calculable from the coupled differential equations of the matter and the dark energy fluctuations:

$$\begin{aligned} \ddot{\delta}_m + 2H\dot{\delta}_m &= 4\pi G(\rho_m\delta_m + \delta\rho_Q + 3\delta p_Q), \\ \ddot{\delta}_Q + 3H\dot{\delta}_Q + \left(k^2 + \frac{d^2V}{dQ^2}\right)\delta_Q &= \dot{\delta}_m [(1+w_Q)\rho_Q]^{1/2} \end{aligned} \quad (16)$$

where $\delta_m = \delta\rho_m/\rho_m$, $\delta_Q = \delta\rho_Q/\rho_Q$ and a dot denotes derivative with respect to proper time. In the limit where the inhomogeneity in Q -fields is negligible, the evolution of δ_m is decoupled from the dark energy fluctuations [34, 35]. In this limit, the influence of dark energy is entirely through $H(z)$.

At $k < \sqrt{|d^2V/dQ^2|}$, δ_Q grows via gravitational instability and will cluster like a matter component. The evolution of δ_m will be affected by δ_Q and will therefore be k -dependent in the era of dark energy domination. At $k > \sqrt{|d^2V/dQ^2|}$, δ_Q is damped out and the evolution of δ_m will be independent of δ_Q . The characteristic scale k_Q of this regime is given by

$$k_Q = 0.001 \sqrt{(1-w) \left(2 + 2w - \frac{w\Omega_m}{\Omega_m + \Omega_Q a^{-3w}} \right)}, \quad (17)$$

where k_Q is in the unit of $h \text{Mpc}^{-1}$ [36].

The characteristic angular wavenumber is given by $l_Q \sim k_Q r(\eta)$ where r is the angular diameter distance and η is conformal time. Assuming our fiducial model, l_Q is around 20 for the CMB shear map and even less for the galaxy source plane shear maps. We therefore restrict our analyses to $l > 40$ where the shear maps will be unaffected by dark energy fluctuations.

Analysis of real data could proceed in two stages. At the first stage, one would fit the data with the modes $l >$

Experiment	f_{sky}	\bar{n}_{tot}	$\bar{n}_{\text{tot}}/\gamma_{\text{rms}}^2$
G4 π	1	65	1900
G2 π	0.5	65	1900
S300	0.0073	100	2920
S1000	0.024	100	2920

TABLE I: Weak lensing experimental parameters assumed. ‘G’ and ‘S’ are for ground- and space-based observations respectively which have different source redshift distributions. Units for the total source sky density, \bar{n}_{tot} , are $1/\text{arcmin}^2$ and the per-component rms intrinsic shear, γ_{rms} , is evaluated at $z = 1$.

Experiment	$l_{\text{max}}^{\text{T}}$	$l_{\text{max}}^{\text{E,B}}$	ν (GHz)	θ_b	Δ_T	Δ_P
Planck	2000	2500	100	9.2’	5.5	∞
			143	7.1’	6	11
			217	5.0’	13	27
CMBpol	2000	2500	217	3.0’	1	1.4

TABLE II: CMB experimental parameters assumed. Planck has more channels which we assume are used entirely for control of foregrounds.

40 where the effect of δQ on matter density perturbations is negligible. With the best-fit w_i determined, one could use interpolation to generate a smooth $w(z)$ as well as the first few eigenmodes of fluctuations about $w(z)$. The amplitudes of these eigenmodes could then be fit to all the data.

IV. EXPERIMENTS

Weak lensing surveys are beginning to make their impact on cosmology [6]. For example, Contaldi et al.[37] find the combination of early Red-Sequence Cluster Survey (RCS) data [38] and WMAP data [2] give $\sigma_8 = 0.89 \pm 0.05$ and $\Omega_m = 0.30 \pm 0.03$. Ongoing surveys of tens to hundreds of square degrees include the Deep Lens Survey (DLS[76]), the Canada-France-Hawaii Telescope Legacy Survey (CFHTLS [77]), the National Optical Astronomy Observatory (NOAO[78]) Deep Wide-Field Survey, and the Red-sequence Cluster Survey (RCS [79]). Longer term there are projects that may cover 1000 square degrees or more. These are the SuperNova Acceleration Probe (SNAP [80]), Pan-STARRS [81] and the Large-aperture Synoptic Survey Telescope (LSST[82]).

We consider two sets of reference surveys, ground-based and space-based which have different total source density and source redshift distributions. For the ground-based surveys we use a galaxy redshift distribution for a limiting magnitude in R of 26 inferred from observations

with the Subaru telescope [39]. The shape of this distribution is well-described by the following analytic form:

$$\begin{aligned} dn/dz &\propto z^{1.3} \exp\left[-(z/1.2)^{1.2}\right] \quad \text{for } z < 1 \\ dn/dz &\propto z^{1.1} \exp\left[-(z/1.2)^{1.2}\right] \quad \text{for } z > 1. \end{aligned} \quad (18)$$

We use this distribution with the modification that half of the galaxies in the $1.2 < z < 2.5$ range are discarded for insufficiently accurate photometric redshifts. The amplitude of the distribution is such that, after this cut, the number density of galaxies is 65 per sq. arcmin[83].

Space-based surveys have the advantage of no sky noise, allowing them to reach higher limiting magnitudes, and the possibility of additional bands in wavelength ranges for which the atmosphere is opaque. The latter advantage means photometric redshifts can be done even in the problematic $1.2 < z < 2.5$ range [40]. For the space-based surveys we assume

$$dn/dz \propto z^2 \exp(-z/1.5) \quad (19)$$

which was also assumed by [21] and which is a close approximation to what was used in a study of the SNAP 300 sq. degree survey [40]. This study predicted a number density of ~ 100 galaxies per sq. arcminute.

The disadvantage of space is that the telescopes are smaller due to the high cost of putting large mirrors in space. This means that ground-based surveys can cover much more sky. Our two ground-based surveys are denoted by G4 π (an all-sky survey) and G2 π (a half-sky survey) and our two space-based surveys are called S1000 and S300 with the numbers denoting the observed area in square degrees. Their properties are summarized in Table I. Baseline plans for LSST include a G2 π survey.

An important quantity for forecasting parameter constraints from *any* cosmic shear observation is γ_{rms} . This quantity is potentially experiment-dependent, with ground-based observations having a higher effective γ_{rms} than space-based ones [40, 41]. But for the low-noise ground-based observations we consider here, γ_{rms} may be just as good as from space. In fact, ground-based observations [42] have achieved very low γ_{rms} . Jarvis et al. [42] find for the lowest-redshift galaxies in their 75 sq. degree CTIO survey that the shape noise contribution to the per-component rms shear, γ_{rms} , is 0.15. The shape noise, as inferred from these data, increases approximately linearly to 0.22 by $z = 2$ [84]. This trend with redshift is also consistent with simulations of SNAP weak lensing observations, based on HDF data, that show γ_{rms} , averaged over all galaxies suitable for ellipticity measurement, increasing from 0.21 to 0.25 with increasing observing time per unit solid angle [40]. We therefore model γ_{rms} as

$$\gamma_{\text{rms}}(z) = 0.15 + 0.035z. \quad (20)$$

Note that other forecasting papers typically assume γ_{rms} of 0.3 or 0.4.

For the CMB experiments we consider Planck [43] and a high-resolution version of CMBpol [85]. Their specifications are given in Table II. We assume that other frequency channels of Planck and CMBpol (not shown in the table) will clean out non-CMB sources of radiation perfectly. Detailed studies have shown foreground degradation of the results expected from Planck to be mild [44, 45, 46]. At $l > 3000$ emission from dusty galaxies will be a significant source of contamination. The effect is expected to be more severe for temperature maps. Hence we restrict temperature data to $l < 2000$ and polarization data to $l < 2500$.

V. ERROR FORECASTING METHOD

The shear two-point functions depend on not just the dark energy parameters, but on the entire matter content and the primordial power spectrum. We do not assume these quantities to be known, but instead assume that CMB data are available to constrain them. The CMB power spectra we include in our analyses are the (unlensed) \tilde{C}_l^{TT} , \tilde{C}_l^{TE} and \tilde{C}_l^{EE} . We do not use the lensed power spectra to avoid the complication of the correlation in their errors between different l values and with the error in the CMB-derived shear power spectrum. Using the lensed spectra and neglecting these correlations can lead to overly optimistic forecasts [7].

To calculate the expected parameter errors we make a first order Taylor expansion of the parameter dependence of all the CMB and cosmic shear two-point functions. In this ‘linear response’ approximation, given the expected experimental errors on the power spectra, we can easily calculate the expected parameter error covariance matrix as the inverse of the Fisher matrix [47]. The linear response approximation is improved and susceptibility to numerical error is reduced with a careful choice of the parameters used to span a given model space [48, 49, 50, 51]. As in [24] we take our (non- $w(z)$) set to be $\mathcal{P} = \{\omega_m, \omega_b, \omega_\nu, \theta_s, z_{\text{ri}}, k^3 P_\Phi^i(k_f), n_s, n'_s, y_{\text{He}}\}$, with the assumption a flat universe. The first three of these are the densities today (in units of $1.88 \times 10^{-29} \text{g/cm}^3$) of cold dark matter plus baryons, baryons and massive neutrinos. We assume two massless species and one massive species. The next is the angular size subtended by the sound horizon on the last-scattering surface. The Thompson scattering optical depth for CMB photons, τ , is parameterized by the redshift of reionization z_{ri} . The primordial potential power spectrum is assumed to be $k^3 P_\Phi^i(k) = k_f^3 P_\Phi^i(k_f) (k/k_f)^{n_s-1+n'_s \ln(k/k_f)}$ with $k_f = 0.05 \text{Mpc}^{-1}$. The fraction of baryonic mass in Helium (which affects the number density of electrons) is y_{He} . We Taylor expand about $\mathcal{P} = \{0.146, 0.021, 0, 0.6, 6.3, 6.4 \times 10^{-11}, 1, 0, 0.24\}$. The Hubble constant for this model is $h = 0.655$ where $H_0 = 100h \text{ km sec}^{-1} \text{ Mpc}^{-1}$.

We follow [52] to calculate the errors expected in \tilde{C}_l^{TT} , \tilde{C}_l^{TE} and \tilde{C}_l^{EE} given Table 1. The errors on the unlensed spectra in the regime where lensing is important (deep in

the damping tail) are certainly underestimated because reconstruction of the unlensed map from the lensed map will add to the errors. However, this is not worrisome since we limit all the unlensed spectra to $l < 2000$.

The contribution to the Fisher matrix from the shear-shear correlations is given by (e.g., [53])

$$F_{pp'}^{\gamma\gamma} = \sum_{l, B_1, B_2, B_3, B_4} \frac{2l+1}{2} C_{l,p}^{B_1, B_2} \mathcal{W}_l^{B_2, B_3} C_{l,p'}^{B_3, B_4} \mathcal{W}_l^{B_4, B_1} \quad (21)$$

where the subscript $,p$ denotes differentiation with respect to parameter a_p . We use \mathcal{W} to denote the inverse of the total covariance matrix:

$$\mathcal{W} \equiv (\mathbf{S} + \mathbf{N})^{-1}. \quad (22)$$

Note that \mathcal{W} is an easily invertible block diagonal matrix: $\mathcal{W}_{lm, B, l' m' B'} = \mathcal{W}_l^{BB'} \delta_{mm'} \delta_{BB'}$. The total Fisher matrix is given by summing $F^{\gamma\gamma}$ with the Fisher matrix for the unlensed CMB data, F^{CMB} .

VI. RESULTS

Above we have described the non- $w(z)$ parameters of our fiducial model, about which we consider small fluctuations. For $w(z)$, we consider two different fiducial cases. Both are constant w models, one with $w_{\text{fid}} = -1$ and the other with $w_{\text{fid}} = -0.8$. About this fiducial model we vary all the cosmological parameters and either w_0 and w_a or the five binned w_i 's.

A. Dependence on Sky Coverage and Shape Noise

First we explore the dependence of constraints on w_0 and w_a as a function of sky coverage and shear weight-per solid angle, $\bar{n}/\gamma_{\text{rms}}^2$. These are both quantities over which the experimenter has some control. The shape of dn/dz is taken to be that assumed for LSST. The left panels of Fig. 2 show the errors on w_0 and w_a assuming $l_{\text{max}} = 1000$. The contours drop rapidly at low $\bar{n}/\gamma_{\text{rms}}^2$ but by $\bar{n}/\gamma_{\text{rms}}^2 = 1000$ the improvement slows dramatically. At such high shear weights, the dominant contribution to the parameter errors comes from sample variance rather than shear noise.

Note that we are only varying the f_{sky} for the cosmic shear observations. We keep the f_{sky} for CMB observations fixed at 1. Therefore the parameter errors reduce more slowly than $f_{\text{sky}}^{1/2}$. The improvement with increasing sky coverage is slowest for w_a which is more dependent on the constraints provided by the CMB observations.

If the non-linearities can be controlled out to $l = 2000$ the errors on w_0 and w_a improve by about 50%. Because the shear angular power spectrum drops with increasing l , the relative importance of shear noise variance to shear sample variance increases with increasing l . Therefore the contours in the right panels of Fig. 2 begin to flatten out at higher values of $\bar{n}_{\text{tot}}/\gamma_{\text{rms}}^2$ than for the $l_{\text{max}} = 1000$ case.

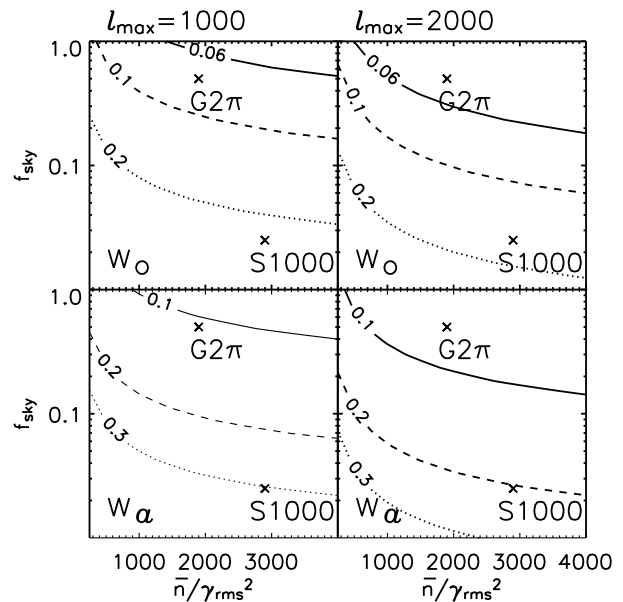


FIG. 2: Contours of constant error in w_0 (top panels) and w_a (bottom panels) for cosmic shear observations of f_{sky} of the sky and shear weight per solid angle $\bar{n}_{\text{tot}}/\gamma_{\text{rms}}^2$. The left panels are for $l_{\text{max}} = 1000$ and the right panels are for $l_{\text{max}} = 2000$. These parameter error forecasts also include constraints from Planck.

B. Dependence on Parameter Space and CMB Experiment

Next we turn to forecasted constraints for w_0 and w_a for the four cosmic shear observations combined with the two CMB observations. First note from Table III that the CMB experiments alone are incapable of constraining these parameters. The primary CMB signal offers no constraint due to the angular-diameter distance degeneracy and CMB lensing only provides a very weak handle since dark energy is only important at very low redshifts, well below the peak of the CMB lensing kernel. The situation improves dramatically with the introduction of the cosmic shear-shear correlations.

Unlike luminosity distances to type-Ia supernovae, cosmic shear power spectra depend on a lot of parameters other than Ω_m , w_0 and w_a . In fact, they depend on all the parameters in our full set except for the optical depth τ . Unfortunately, the spectra are nearly featureless and therefore incapable of simultaneously fitting this large number of parameters. Thus the CMB measurements are key to breaking the degeneracies.

The degeneracy-breaking provided by the CMB is highly effective. Forecasts for errors on the $w(z)$ parameters, assuming everything else is fixed by Planck, are fairly accurate as long as they include one more parameter to be determined by cosmic shear data. As shown at the bottom of Table III, this parameter could be θ_s or

TABLE III:

CMB	Cosmic Shear	w_0	w_a	m_ν	$\ln \Omega_m h^2$	$\ln P_\Phi$	n_S	n'_S	τ	$\ln \omega_b$	Y_P	θ_s
Planck	none	2.2	3.3	0.18	0.0084	0.017	0.0078	0.0035	0.010	0.0086	0.013	0.00016
none	G4 π	0.012	0.020	—	—	—	—	—	—	—	—	—
		0.051	0.066	—	0.00089	—	—	—	—	—	—	—
		0.051	0.069	—	—	—	—	—	—	—	—	0.00027
Planck	S300	0.41	0.49	0.12	0.0068	0.016	0.0066	0.0034	0.0091	0.0076	0.011	0.00014
	S1000	0.28	0.34	0.090	0.0059	0.015	0.0060	0.0033	0.0090	0.0069	0.011	0.00014
	G2 π	0.076	0.11	0.052	0.0039	0.014	0.0046	0.0029	0.0083	0.0059	0.0094	0.00012
	G4 π	0.056	0.087	0.045	0.0035	0.013	0.0044	0.0025	0.0077	0.0058	0.0087	0.00012
Planck	G4 π	0.049	0.063	—	0.00083	—	—	—	—	—	—	—
		0.021	0.031	—	—	—	—	—	—	—	—	9.4×10^{-5}
		0.050	0.064	—	0.00086	—	—	—	—	—	—	9.7×10^{-5}
		0.050	0.065	0.018	0.0015	—	—	—	—	—	—	9.8×10^{-5}
		0.050	0.069	0.018	0.0028	0.0093	—	—	0.0055	—	—	0.00011
		0.051	0.070	0.020	0.0033	0.011	0.0020	—	0.0070	—	—	0.00011
		0.052	0.074	0.023	0.0033	0.011	0.0020	0.0019	0.0070	—	—	0.00011
CMBpol	none	0.79	1.1	0.048	0.0040	0.017	0.0031	0.0018	0.0097	0.0028	0.0048	4.8×10^{-5}
	S300	0.18	0.24	0.047	0.0038	0.012	0.0029	0.0018	0.0073	0.0028	0.0047	4.6×10^{-5}
	S1000	0.13	0.17	0.045	0.0036	0.011	0.0028	0.0018	0.0069	0.0028	0.0046	4.6×10^{-5}
	G2 π	0.064	0.089	0.031	0.0026	0.0099	0.0026	0.0016	0.0060	0.0027	0.0044	4.2×10^{-5}
	G4 π	0.049	0.070	0.027	0.0023	0.0093	0.0025	0.0015	0.0057	0.0026	0.0043	4.1×10^{-5}

NOTES.—Forecasts of 1- σ errors for the combination of tomographic shear-shear two-point functions with Planck and CMBpol. A ‘—’ indicates a parameter held fixed.

$\Omega_m h^2$. However, assuming that Planck determines both θ_s and $\Omega_m h^2$ perfectly well results in overly optimistic forecasts for w_0 and w_a . This is a bit surprising since the CMB does such an exquisite job on both θ_s and $\Omega_m h^2$. The reason for it is that the shear power spectra are highly sensitive to the shape parameter, $\Omega_m h$ which is a combination of θ_s and $\Omega_m h^2$. Even very small uncertainties in $\Omega_m h$ can significantly increase the errors on w_0 and w_a .

Replacing Planck with four-year WMAP, the error forecasts for w_0 and w_a from G4 π weaken from 0.056 to 0.064 and from 0.087 to 0.11 respectively. Replacing Planck with CMBpol, as we see in Table III, strengthens the constraint to the limit of all parameters (other than w_0 , w_a and either θ_s or $\Omega_m h^2$) being fixed by the CMB.

C. Neutrino Mass

Replacing a massless neutrino species with a massive one increases the energy density and therefore the expansion rate, suppressing the growth of structure. The suppression of the power spectrum is scale dependent and the relevant length scale is the Jeans length for neutrinos [54, 55, 56] which decreases with time as the neutrino thermal velocity decreases. This suppression of growth is ameliorated at scales larger than the Jeans length at

matter–radiation equality, where the neutrinos can cluster. Neutrinos never cluster at scales smaller than the Jeans length today. The net result is no effect on scales larger than the Jeans length at matter–radiation equality and a scale-independent suppression of power on scales smaller than the Jeans length today. Both the total suppression of power and the Jeans length today depend on the neutrino mass.

The observed galaxy power spectrum (which is proportional to the matter power spectrum at sufficiently large scales), combined with CMB observations can be used to put constraints on m_ν [57]. At present such an analysis yields an upper bound on m_ν of ~ 0.3 eV [58].

Since the shear power spectra depend on the history of the matter power spectrum they can also be used to determine neutrino masses. Recently, [24] showed that an experiment with the specifications of CMBpol in Table II could determine the mass of a relic neutrino species via its effect on the lensing of the cosmic microwave background with an uncertainty of 0.044 eV. This analysis assumed a time-independent w . We see in Table III that allowing for variation of w_a weakens the neutrino constraint only slightly to 0.048 eV. A reasonable prior on w_0 and w_a would eliminate this degradation.

Adding constraints from shear-shear correlations to CMBpol only improves the neutrino mass constraints by less than a factor of 2. We will see more dramatic im-

provement with the introduction of the ratio statistic in the next section. Shear-shear correlations make a more dramatic improvement for m_ν when added to Planck. The combination of Planck and G2 π does nearly as well as CMBpol alone. A similar result was found in [22, 23], although with the assumption of $w = -1$.

D. Primordial Power Spectrum Parameters

One of the virtues of inflation is the robustness and simplicity of its predictions. On the other hand, this robustness and simplicity make it difficult to probe observationally in detail. One of the few observational handles we have is the shape of the primordial power spectrum. High-precision determination of n_S and (even better) determination of non-zero $n'_S \equiv dn_S/d\ln k$ would be highly valuable information about inflation or whatever mechanism generated the initial fluctuations.

Recently the scalar power spectrum has been a subject of great interest due to claims of non-zero n'_S . The evidence from CMB data alone is very weak: $n'_S \equiv dn_S/d\ln k = -0.055 \pm 0.038$ [58]. Combining CMB data with the Croft et al. matter power spectrum inferred from high-resolution observations of the Ly α forest results in $n'_S = -0.031 \pm 0.017$ [58]. Other authors [59] working with the same datasets though have since found looser constraints when they marginalize over the mean ionizing flux as a function of redshift. The importance of marginalizing over this parameter, which leads to a large degeneracy between spectral index and amplitude, was pointed out in [60].

Progress in studying the scalar power spectrum is likely to come mostly from higher-resolution CMB experiments. As we can see in Table III (and in [24]) Planck will improve the constraints on n'_S from current values by a factor of 10. If the error bars shrink around the current best-fit values, this improved precision will have profound implications since such large departures from scale-invariance are not expected in inflationary models.

The difference $n_S - 1$ is first order in the slow-roll parameters and n'_S is second order. Thus we expect $|n'_S|$ to be on the order of $(n_S - 1)^2$. If $1 - n_S = 0.03$, which is perfectly consistent with present data, then we would expect to see non-zero n'_S at about the 10^{-3} level. It would be tremendously exciting to actually confirm this expectation. Note though that there are models with $|n'_S| \sim n_S - 1$ [61] so this is not a firm test. Nevertheless, finding $\sigma(n'_S) \gg n_S - 1$ would be difficult to reconcile with inflation [61].

Confirming the expectation that $n_S - 1$ is on the order of $(n_S - 1)^2$ is likely to take the precision of CMBpol, as pointed out in [24]. Unfortunately, even if $1 - n_S$ is as large as 0.06, CMBpol alone would still only achieve a two-sigma detection of $n'_S = (n_S - 1)^2$. Further, the addition of cosmic shear to CMBpol does not improve the constraints on n'_S by much, although it can improve $\sigma(n'_S)$ by a factor of five over what's possible with WMAP

data alone [62].

It is very hard to imagine what could improve the determination of n'_S further [63]. Extending dynamic range further only improves the error logarithmically, and then only if power at the smaller scale is measured with precision comparable to that at the larger scale. It is highly unlikely that systematics on any small-scale measurement could be controlled well enough to result in constraints on the primordial power spectrum amplitude at the 10^{-3} level.

Finally, note that the amplitude of the primordial power spectrum is better-determined with the addition of cosmic shear. And since the CMB determines $P_\Phi \exp(-2\tau)$ to very high accuracy, the τ constraint improves too [7].

E. Dark Energy Tomography

Now we turn to the results for the discrete parametrization of $w(z)$, shown in Fig. 3 and Fig. 4. We see that the errors grow with increasing redshift as expected due to the decreasing importance of dark energy with increasing redshift. For $w = -1$, matter-dark energy equality is at $z_{eq} \simeq 0.25$. The percentages of the total density in dark energy are 25%, 7% and 3% at $z = 1$, $z = 2$ and $z = 3$ respectively. For $w = -0.8$ the drop off is slower so the rise in the errors is slower. The highest-redshift bin is the broadest bin, stretching from $z = 1.6$ all the way to $z = 1100$; this width is responsible for the smaller error in the highest redshift bin.

We see from Fig. 3 and Fig. 4 that weak lensing observations of very large amounts of sky will allow for a reconstruction of $w(z)$ up to $z = 2$, with errors in all five bins (for the G4 π , $w_{fid} = -0.8$ case) less than 0.2.

The smaller sky coverage of the space-based surveys leads to much worse constraints. Although here we must remind the reader that we are focusing on science that can be done with information on the larger angular scales. Space-based observations will have advantages with respect to ground-based observations at smaller angular scales.

The errors in w_i are highly correlated. It is useful for us to find an uncorrelated linear combination of w_i when we fit the large scale modes at the second stage. We write $\tilde{w}_\alpha = R_{\alpha i} w_i$ and find $R_{\alpha i}$ such that

$$\begin{aligned} \langle \Delta \tilde{w}_\alpha \Delta \tilde{w}_\beta \rangle &= \tilde{F}_{\alpha\beta}^{-1} = E_\alpha^2 \delta_{\alpha\beta} \\ &= \sum_{i,j=1}^5 R_{\alpha i} F_{ij}^{-1} R_{j\beta} \end{aligned} \quad (23)$$

where $\tilde{F}_{\alpha\beta}^{-1}$ is the (diagonal) Fisher matrix for the transformed parameters and the transformation matrix R satisfies $R_{\alpha i} R_{i\beta}^T = \delta_{\alpha\beta}$. TABLE IV shows 1- σ errors for the amplitudes of the eigenmodes of w_i .

After the first stage of analysis, restricted to $l > 40$ and ignoring dark energy fluctuations, one would proceed to

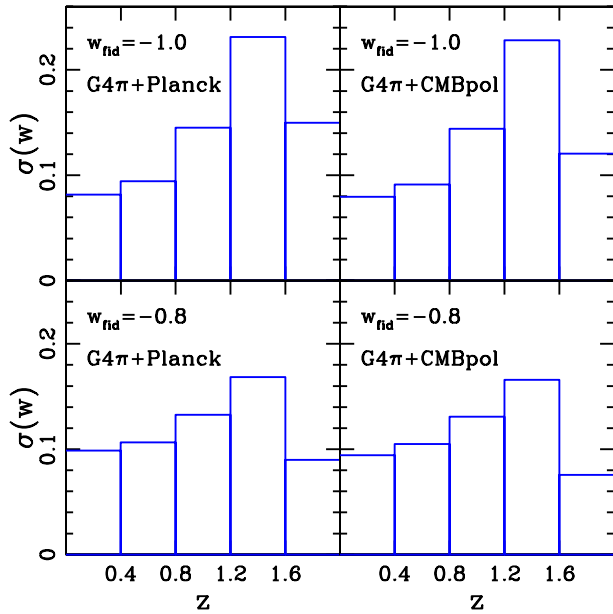


FIG. 3: Error boxes indicate expected $1\text{-}\sigma$ error in each w_i for $G4\pi$ combined with either Planck (left panels) or CMBpol (right panels) for $w_{\text{fid}} = -1$ (top panels) or -0.8 (bottom panels).

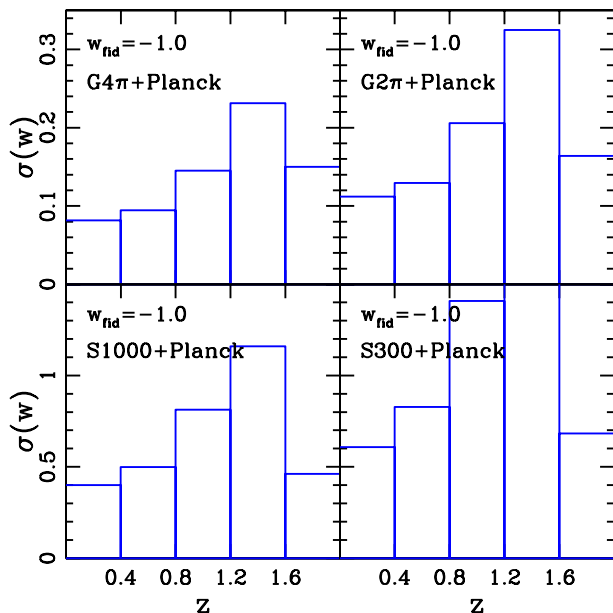


FIG. 4: Error boxes indicate expected $1\text{-}\sigma$ error in each w_i for the combination of experiments specified in each panel.

E1	E2	E3	E4	E5
0.021	0.046	0.088	0.13	0.28

TABLE IV: Forecasts for $1\text{-}\sigma$ errors on the w_i eigenmode amplitudes for $G4\pi$ and CMBpol assuming $w_{\text{fid}} = -1$.

a second stage which would extend to larger scales and take the fluctuations into account. The second stage of analysis would use a smoothed version of the eigenmodes derived from the first stage of analysis as the basis for the parametrization of $w(z)$. We can test the consistency from what we found at the first stage, though we do not expect noticeable improvement at the second stage. Because the large-scale and small-scale data are uncorrelated, the small-scale data could simply be included as a prior determined in the first stage of the analysis. Including the small-scale data in this way may be of practical use, in terms of making the data analysis tractable, if the parameter space needs to be broadened to include the sound-speed of the dark energy. For a study of how well the sound speed can be constrained see [7].

VII. THE RATIO STATISTIC

We have restricted our use of the shear maps to $l < 1000$ to reduce our sensitivity to theoretical errors in the calculation of $P(k, z)$. The density power spectrum is difficult to calculate on small scales where the influence of baryons becomes important.

However, discarding the data at $l > 1000$ is highly unfortunate since there is tremendous signal-to-noise on these angular scales, as can be seen in Fig. 1. Recently Jain & Taylor [20] proposed a ratio statistic that uses this small-scale data to constrain cosmology, but that is not biased by errors in the small-scale power spectrum. Here we combine the ratio statistic with the shear-shear power spectra at $l < 1000$ and find it provides highly complementary constraints on the bins of w .

Further details on how the Jain & Taylor idea [20] might be implemented are given in Bernstein & Jain [21]. They write the observed eccentricity as

$$\mathbf{e}_k^{\text{obs}} = \sum_l d_l(\mathbf{x}_k) g_{lk} + \mathbf{e}_k. \quad (24)$$

The distortion field d_l is the distortion field for sources at infinity due to mass inside redshift shell l . The g_{lk} is a purely geometric term that corrects the distortion for a source at finite distance r_k . If the distortion field is dominated by a single lensing object then we can write

$$\mathbf{e}_k^{\text{obs}} = d_{l^*}(\mathbf{x}_k) g_{l^*k} + \sum_{l \neq l^*} d_l(\mathbf{x}_k) g_{lk} + \mathbf{e}_k \quad (25)$$

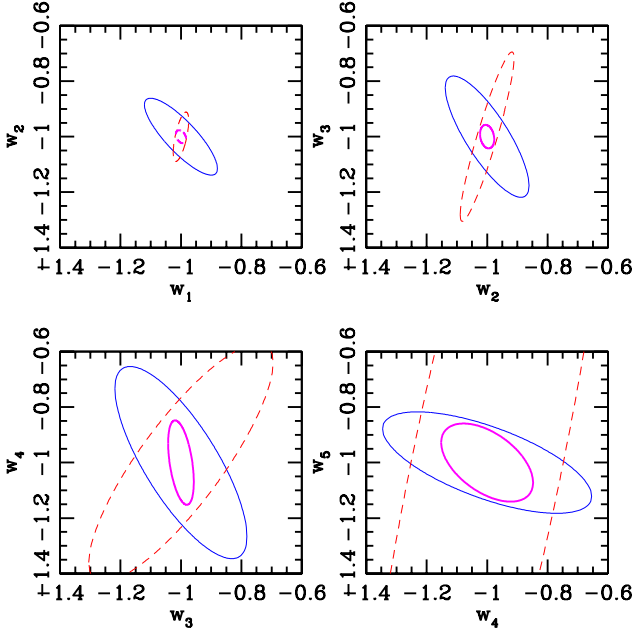


FIG. 5: Forecasts of $1\text{-}\sigma$ error contours for pairs of w_i assuming G4 π and CMBpol. The thin solid contour is for shear-shear correlations alone, the dashed contour is for the ratio statistic alone and the thick contour is for their combination.

which is just rewriting the above, but with the understanding that the term with the sum is now small compared to the others. With the assumption of a shape for the distortion field, $d_{l*}(\mathbf{x}_k)$, one can determine g_{l*k} up to a normalizing constant, as well as $g_{l*k'}$ up to the same normalizing constant. Thus Jain and Taylor proposed using the ratio of such determinations to give a purely geometric quantity. This is their ratio statistic. Its expectation value is

$$R_{kk'}^l = g_{lk}/g_{lk'}. \quad (26)$$

A rough idea of how well $R_{kk'}^l$ can be determined is given by considering the typical amplitude of the shear signal and the area over which it can be measured, the latter affecting how many galaxies can be used to beat down shape noise. This leads to

$$\begin{aligned} C_{kk',jj'}^l &\equiv \left\langle \frac{\Delta R_{kk'}^l}{R_{kk'}^l} \frac{\Delta R_{jj'}^l}{R_{jj'}^l} \right\rangle \\ &\simeq \frac{\langle n_k^2 \rangle}{\gamma_k^l \gamma_j^l} \delta_{kj} + \frac{\langle n_{k'}^2 \rangle}{\gamma_{k'}^l \gamma_{j'}^l} \delta_{k'j'} \end{aligned} \quad (27)$$

where γ_k^l is the average amplitude of the tangential shear of galaxies in source bin k due to lenses in lens slice l . The noise variance $\langle n_k^2 \rangle$ is given by

$$\langle n_k^2 \rangle \simeq \frac{\gamma_{\text{rms}}^2}{N_k f_l} \quad (28)$$

where f_l denotes the fraction of the sky covered by templates for lenses in lens redshift slice l .

To proceed further we need estimates for the shear template amplitudes γ_k^l and the fraction of the sky in the observed regions covered by the templates, f_l . Jain & Taylor [20] point out that the number density of clusters with mass in a logarithmic interval about $m = 10^{14} M_\odot$ out to $z = 1$ is $0.01/\text{arcmin}^2$. Further, for a galaxy cluster of this mass at $z = 0.2$ with lens source at $z = 1$ the tangential shear signal is nearly constant out to $1'$ with an area-weighted average amplitude of about 0.05 [64]. We therefore set $\gamma_k^l = 0.05$ and define the area useable for estimating the template amplitude to be that within the $1'$ radius. With this template area per object and considering objects with masses in the decade surrounding $m = 10^{14} M_\odot$ we get a fraction of the observing area covered with templates of about 0.06. Dividing this into three lens slices (centered on $z = 0.2$, $z = 0.6$ and $z = 1$) we get $f_l = 0.02$.

Jain and Taylor[20] used a full halo model calculation of the signals expected and area that could be used for measuring them in each lens slice for each mass of cluster in order to forecast errors on their ratio statistic, and therefore on dark energy parameters. They also used a version of the simple forecast above that was able to reproduce the results of their more detailed calculation. Our simple forecast for errors on the ratio statistic is much more conservative than theirs. The main difference is that they assumed an area with a radius of $3'$ about each cluster could be used for measuring the shear template amplitude. We chose the smaller radius to reduce contamination from projection.

Our results including lensing cosmography are more speculative than our results from just CMB and the shear two-point functions. Projection effects may be important, even with our restriction to $1'$. Although [21] included projection effects, they did so with a halo model calculation which may be inadequate for this purpose given its assumption of spherical halos. Further, the construction of templates from the galaxy distribution may not be as robust as assumed in [21]. Numerical simulations could address the projection problem [19]. Finally, unlike the sample-variance dominated shear-shear correlation statistics, the errors we forecast on the ratio statistic depend strongly on the achievement of the low level of shape noise that we assume.

The Fisher matrix for the ratio statistic is given by

$$F_{pp'}^R = \sum_l \sum_{kk'} \frac{R_{kk',p}^l}{R_{kk'}^l} C_{kk',kk'}^{l-1} \frac{R_{kk',p'}^l}{R_{kk'}^l} \quad (29)$$

where we have approximated the C matrix to be independent of cosmological parameters. We calculate this Fisher matrix summing over the three lens planes and all eight cosmic shear source planes. Because the ratio statistic is influenced by data on smaller angular scales than the shear-shear statistics (since there we restricted to $l < 1000$) the errors are independent and the Fisher

TABLE V:

CMB	Cosmic Shear	w_0	w_a	m_ν	$\ln \Omega_m h^2$	$\ln P_\Phi$	n_S	n'_S	τ	$\ln \omega_b$	Y_P	θ_s
Planck	none	2.2	3.3	0.18	0.0084	0.017	0.0078	0.0035	0.010	0.0086	0.013	0.00016
	S300	0.16	0.26	0.074	0.0061	0.015	0.0065	0.0033	0.0090	0.0073	0.011	0.00014
	S1000	0.10	0.16	0.051	0.0048	0.015	0.0058	0.0031	0.0089	0.0067	0.011	0.00014
	G2 π	0.031	0.053	0.019	0.0033	0.014	0.0037	0.0020	0.0080	0.0058	0.0067	0.00012
	G4 π	0.022	0.040	0.014	0.0030	0.013	0.0033	0.0017	0.0074	0.0056	0.0059	0.00011
CMBpol	none	0.79	1.1	0.048	0.0040	0.017	0.0031	0.0018	0.0097	0.0028	0.0048	4.8×10^{-5}
	S300	0.12	0.20	0.044	0.0036	0.012	0.0029	0.0018	0.0073	0.0028	0.0046	4.6×10^{-5}
	S1000	0.082	0.13	0.037	0.0033	0.011	0.0028	0.0018	0.0066	0.0028	0.0046	4.5×10^{-5}
	G2 π	0.028	0.047	0.017	0.0022	0.0086	0.0024	0.0014	0.0053	0.0026	0.0037	3.9×10^{-5}
	G4 π	0.021	0.035	0.013	0.0021	0.0080	0.0021	0.0013	0.0049	0.0025	0.0033	3.6×10^{-5}

NOTES.—Forecasts of $1\text{-}\sigma$ errors for the combination of tomographic shear-shear two-point functions and the ratio statistic with Planck (upper table) and CMBpol (lower table).

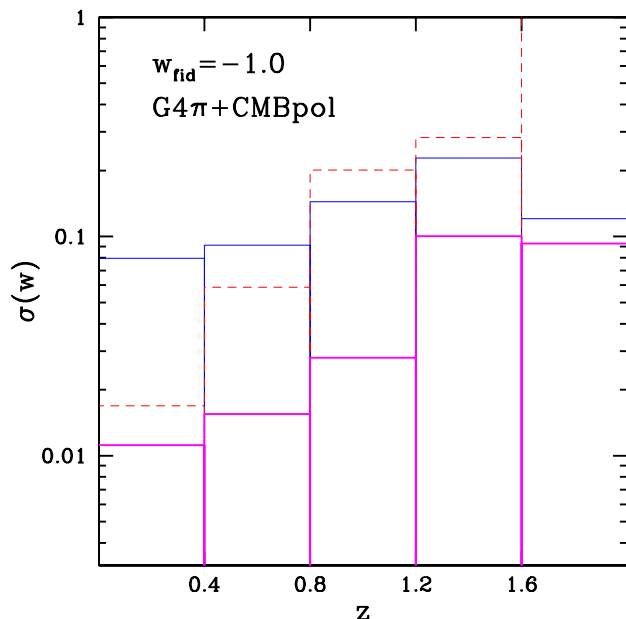


FIG. 6: Forecasts of $1\text{-}\sigma$ errors in w_i for the $i = 1$ to 5 redshift bins for CMBpol combined with the all-sky weak lensing experiment G4 π . The thin solid error boxes are for shear-shear correlations alone, the dash error boxes are for the ratio statistic alone and the thick solid boxes are for the combination.

matrices simply add:

$$F_{pp'} = F_{pp'}^{\gamma\gamma} + F_{pp'}^R + F_{pp'}^{\text{CMB}}. \quad (30)$$

Despite our more conservative treatment, we still find the ratio statistic to provide a powerful constraint on dark energy especially when combined with the shear-shear correlations investigated above. Parameter error forecasts for the two-parameter dark energy model from

combining shear-shear correlations and the ratio statistic with CMB data are shown in Table V. We see that the addition of the ratio statistic reduces errors in the dark energy parameters by about a factor of two. Constraints on neutrino mass also improve by factors of two and three.

Even more dramatic improvements occur in the w_i space. The combination of shear-shear correlations and the ratio statistic dramatically reduces the degeneracies of these parameters. Fig. 5 shows that with shear-shear correlations the errors in w_i and w_{i+1} are anti-correlated while with the ratio statistic the errors are positively correlated. The result for the combination is a large reduction of the error for each w_i as can be seen in Fig. 6. As is shown in Fig. 6, G4 π plus CMBpol can reconstruct $w(z)$ with uncertainty $\sigma(w_i) \lesssim 0.1$ up to $z \sim 2$.

The anti-correlation from shear-shear correlations is expected since a positive variation of w_i can be compensated for by a negative variation of w_{i+1} . But the complicated ratio statistic leads to the unusual positive correlation, where a positive variation of w_i can be partially compensated for by a positive variation in w_{i+1} .

VIII. DISCUSSION AND CONCLUSIONS

The statistical properties of the large-scale density field are sensitive to the dark energy equation of state. Tomographic cosmic shear observations on large angular scales offer a theoretically robust means of taking advantage of this dependence. While the statistical properties are also sensitive to other matter components and the primordial power spectra, in combination with CMB observations dark energy parameters can still be precisely measured despite these other degrees of freedom.

We have seen that very tight constraints can be achieved on the parameters of an 11-dimensional space,

including the equation-of-state parameter and its time variation, the mass of the relic neutrinos, and the shape and amplitude of the primordial power spectrum. Cosmic shear surveys are critical to the dark energy constraints, and contribute significantly to the other constraints, especially those on neutrino mass.

To explore the constraints possible on the history of the dark energy equation-of-state parameter we introduced a discrete parametrization of $w(z)$. The combination of all-sky weak lensing observations on large angular scales and all-sky CMB observations can constrain w in each of five bands (four evenly spaced from 0 to 1.6 and one from 1.6 to last-scattering) to better than 0.2.

Such precision on w out to redshifts where the dark energy density is subdominant may prove to be highly illuminating as to the nature of the dark energy. Some attractor solutions predict a sharp transition of w from $w \gtrsim 0$ to $w = -1$ at a redshift where the dark energy density is still subdominant [65, 66, 67]. If such a transition happens at $z < 2$, then we can probe that transition point with the binned w_i .

While we have focused on what is possible with the statistical properties that can be most robustly predicted from theory, there is much signal to noise at smaller angular scales. Further work is needed to make full use of these data where non-linear corrections are large. We studied one means of including information from small-scales, the ratio statistic of [20], and found it resulted in large reductions in forecasted parameter errors. The m_ν constraint for G4 π +Planck improved by a factor of three to the very interesting level of 0.014 eV. The G4 π

+ CMBpol constraints on the w_i improved even more dramatically in the three lowest redshift bins.

Many challenges remain to the achievement of the parameter errors we forecast here. We have assumed that residuals from fitting anisotropic point-spread functions, distortions introduced by the camera, photometric redshift errors, redshift-dependent calibration errors [68] and intrinsic alignments [69, 70, 71, 72, 73, 74] are negligible. The validity of these assumptions depends on the skill of the experimenters and analysts and to some degree on the kindness of nature. Study of the impact of these non-idealities and how to tackle them is on-going. Calibration errors of 5%, achievable with current data analysis methods [68], lead to only small changes in forecasted parameter errors [62]. Intrinsic alignment contamination can be avoided by using photometrically-determined redshifts to exclude spatially-close galaxy pairs[86] or, more radically, by restricting analysis to shear cross-spectra and ignoring the auto spectra [75]. Avoiding significant biases in photometric redshifts will require calibration with large, but achievable, numbers of spectroscopic redshifts [21].

IX. ACKNOWLEDGMENTS

We thank Neal Dalal, Joseph Hennawi, Wayne Hu, Bhuvnesh Jain, Manoj Kaplinghat, Lori Lubin, Albert Stebbins, Masahiro Takada, J. Anthony Tyson and David Wittman for useful discussions. This work was supported by NASA grant NAG5-11098 and the NSF.

-
- [1] S. Dodelson and L. Knox, *Physical Review Letters* **84**, 3523 (2000).
 - [2] C. L. Bennett, M. Halpern, G. Hinshaw, N. Jarosik, A. Kogut, M. Limon, S. S. Meyer, L. Page, D. N. Spergel, G. S. Tucker, et al. (2003), astro-ph/0302207.
 - [3] A. G. Riess, A. V. Filippenko, P. Challis, A. Clocchiatti, A. Diercks, P. M. Garnavich, R. L. Gilliland, C. J. Hogan, S. Jha, R. P. Kirshner, et al., *Astron. J.* **116**, 1009 (1998).
 - [4] S. Perlmutter, M. S. Turner, and M. White, *Physical Review Letters* **83**, 670 (1999).
 - [5] S. Perlmutter and SNAP Collaboration, *Bulletin of the American Astronomical Society* **32**, 1504 (2000).
 - [6] L. Van Waerbeke and Y. Mellier, *ArXiv Astrophysics e-prints* (2003), astro-ph/0305089.
 - [7] W. Hu, *Phys. Rev. D* **65**, 23003 (2002).
 - [8] W. Hu and T. Okamoto, *Astrophys. J.* **574**, 566 (2002).
 - [9] D. Huterer, *Phys. Rev. D* **65**, 63001 (2002).
 - [10] A. Refregier, R. Massey, J. Rhodes, R. Ellis, J. Albert, D. Bacon, G. Bernstein, T. McKay, and S. Perlmutter, *ArXiv Astrophysics e-prints* (2003), astro-ph/0304419.
 - [11] M. Takada and B. Jain, *ArXiv Astrophysics e-prints* (2003), astro-ph/0304034.
 - [12] K. Abazajian and S. Dodelson, *Physical Review Letters* **91**, 41301 (2003).
 - [13] A. Heavens, *ArXiv Astrophysics e-prints* pp. 4151+ (2003).
 - [14] K. Benabed and L. Van Waerbeke, *ArXiv Astrophysics e-prints* (2003), astro-ph/0306033.
 - [15] P. Simon, L. J. King, and P. Schneider, *ArXiv Astrophysics e-prints* (2003), astro-ph/0309032.
 - [16] E. V. Linder, *ArXiv Astrophysics e-prints* (2002), astro-ph/0200217.
 - [17] J. Weller and A. Albrecht, *Physical Review Letters* **86**, 1939 (2001).
 - [18] D. Huterer and G. Starkman, *Physical Review Letters* **90**, 31301 (2003).
 - [19] J. A. Tyson, D. M. Wittman, J. F. Hennawi, and D. N. Spergel (2002), astro-ph/0209632.
 - [20] B. Jain and A. Taylor, *ArXiv Astrophysics e-prints* (2003), astro-ph/0306046.
 - [21] G. M. Bernstein and B. Jain, *ArXiv Astrophysics e-prints* (2003), astro-ph/0309332.
 - [22] W. Hu, *ApJ* **522**, L21 (1999).
 - [23] W. Hu, **522**, L21 (1999).
 - [24] M. Kaplinghat, L. Knox, and Y. Song, *ArXiv Astrophysics e-prints* pp. 3344+ (2003).
 - [25] J. F. Beacom and N. F. Bell, *Phys. Rev. D* **65**, 113009 (2002).
 - [26] N. Kaiser, *Astrophys. J.* **388**, 272 (1992).
 - [27] M. Bartelmann and P. Schneider, *Phys. Rep.* **340**, 291 (2001).
 - [28] M. Kamionkowski, A. Kosowsky, and A. Stebbins, *Phys.*

- Rev. Lett. **78**, 2058 (1997).
- [29] U. . Seljak and M. Zaldarriaga, Phys. Rev. Lett. **78**, 2054 (1997).
- [30] J. A. Peacock and S. J. Dodds, MNRAS **267**, 1020 (1994).
- [31] R. Scoccimarro, M. Zaldarriaga, and L. Hui, Astrophys. J. **527**, 1 (1999).
- [32] W. Hu and T. Okamoto, **574**, 566 (2002).
- [33] C. M. Hirata and U. Seljak, ArXiv Astrophysics e-prints (2003), astro-ph/0306354.
- [34] K. Coble, S. Dodelson, and J. A. Frieman, Phys. Rev. D **55**, 1851 (1997).
- [35] R. R. Caldwell, R. Dave, and P. J. Steinhardt, Physical Review Letters **80**, 1582 (1998).
- [36] C. Ma, R. R. Caldwell, P. Bode, and L. Wang, ApJ **521**, L1 (1999).
- [37] C. R. Contaldi, H. Hoekstra, and A. Lewis, Physical Review Letters **90**, 221303 (2003).
- [38] H. Hoekstra, H. K. C. Yee, and M. D. Gladders, Astrophys. J. **577**, 595 (2002).
- [39] M. Nagashima, Y. Yoshii, T. Totani, and N. Gouda, ArXiv Astrophysics e-prints pp. 7483+ (2002).
- [40] R. Massey, J. Rhodes, A. Refregier, J. Albert, D. Bacon, G. Bernstein, R. Ellis, B. Jain, T. McKay, S. Perlmutter, et al., ArXiv Astrophysics e-prints (2003), astro-ph/0304418.
- [41] N. Kaiser, Astrophys. J. **498**, 26+ (1998).
- [42] M. Jarvis, G. M. Bernstein, P. Fischer, D. Smith, B. Jain, J. A. Tyson, and D. Wittman, Astron. J. **125**, 1014 (2003).
- [43] J. A. Tauber, in *IAU Symposium* (2001), pp. 493+.
- [44] L. Knox, MNRAS **307**, 977 (1999).
- [45] M. Tegmark, D. J. Eisenstein, W. Hu, and A. de Oliveira-Costa, Astrophys. J. **530**, 133 (2000).
- [46] F. R. Bouchet and R. Gispert, New Astronomy **4**, 443 (1999).
- [47] G. Jungman, M. Kamionkowski, A. Kosowsky, and D. N. Spergel, Phys. Rev. D **54**, 1332 (1996).
- [48] D. J. Eisenstein, W. Hu, and M. Tegmark, Astrophys. J. **518**, 2 (1999).
- [49] G. Efstathiou and J. R. Bond, **304**, 75 (1999).
- [50] W. Hu, M. Fukugita, M. Zaldarriaga, and M. Tegmark, Astrophys. J. **549**, 669 (2001).
- [51] A. Kosowsky, M. Milosavljevic, and R. Jimenez, Phys. Rev. D **66**, 63007 (2002).
- [52] M. Zaldarriaga, D. N. Spergel, and U. Seljak, Astrophys. J. **488**, 1+ (1997).
- [53] L. Knox, A. Cooray, D. Eisenstein, and Z. Haiman, Astrophys. J. **550**, 7 (2001).
- [54] J. R. Bond and A. S. Szalay, Astrophys. J. **274**, 443 (1983).
- [55] C. Ma, Astrophys. J. **471**, 13 (1996).
- [56] W. Hu and D. J. Eisenstein, Astrophys. J. **498**, 497 (1998).
- [57] W. Hu, D. J. Eisenstein, and M. Tegmark, Phys. Rev. Lett. **80**, 5255 (1998).
- [58] D. N. Spergel et al. (2003), astro-ph/0302209.
- [59] U. Seljak, P. McDonald, and A. Makarov, ArXiv Astrophysics e-prints pp. 2571+ (2003).
- [60] M. Zaldarriaga, L. Hui, and M. Tegmark, Astrophys. J. **557**, 519 (2001).
- [61] B. Gold and A. Albrecht, ArXiv Astrophysics e-prints (2003), astro-ph/0301050.
- [62] M. Ishak, C. M. Hirata, P. McDonald, and U. Seljak, ArXiv Astrophysics e-prints (2003), astro-ph/0308446.
- [63] L. Knox, ArXiv Astrophysics e-prints pp. 4370+ (2003).
- [64] M. Takada and B. Jain, ArXiv Astrophysics e-prints (2003), astro-ph/0310125.
- [65] A. Albrecht and C. Skordis, Physical Review Letters **84**, 2076 (2000).
- [66] C. Armendariz-Picon, V. Mukhanov, and P. J. Steinhardt, Physical Review Letters **85**, 4438 (2000).
- [67] G. R. Farrar and P. J. E. Peebles, ArXiv Astrophysics e-prints (2003), astro-ph/0307316.
- [68] C. Hirata and U. Seljak, **343**, 459 (2003).
- [69] A. Heavens, A. Refregier, and C. Heymans, **319**, 649 (2000).
- [70] P. Catelan, M. Kamionkowski, and R. D. Blandford, **320**, L7 (2001).
- [71] R. G. Crittenden, P. Natarajan, U. Pen, and T. Theuns, Astrophys. J. **559**, 552 (2001).
- [72] U. Pen, J. Lee, and U. Seljak, **543**, L107 (2000).
- [73] J. Mackey, M. White, and M. Kamionkowski, **332**, 788 (2002).
- [74] Y. P. Jing, **335**, L89 (2002).
- [75] M. Takada and M. White, ArXiv Astrophysics e-prints (2003), astro-ph/0311104.
- [76] The Deep Lens Survey
<http://dls.bell-labs.com/>
- [77] <http://www.cfht.hawaii.edu/Science/CFHLS/>
- [78] <http://www.noao.edu/noao/noaodeep/>
- [79] <http://www.astro.utoronto.ca/~gladders/RCS/>
- [80] <http://snap.lbl.gov/>
- [81] The Panoramic Survey Telescope & Rapid Response System (28,000 square degrees)
<http://pan-starrs.ifa.hawaii.edu/>
- [82] <http://www.lsst.org>
- [83] J.A. Tyson, private communication
- [84] D. Wittman, private communication.
- [85] CMBpol: <http://spacescience.nasa.gov/missions/concepts.htm>.
- [86] J.A. Tyson, private communication